1

2

3

4 **The antimicrobial effects of the alginate oligomer OligoG CF-5/20 are independent of direct**

5 **bacterial cell membrane disruption**

6

7 Manon F. Pritchard*[1]; Lydia C. Powell[1]; Saira Khan[1]; Peter C. Griffiths[2]; Omar T. Mansour[2]; Ralf

8 Schweins[3]; Konrad Beck[1]; Niklaas J. Buurma[4]; Christopher E. Dempsey[5]; Chris J. Wright[6]; Philip D.

9 Rye[7]; Katja E. Hill[1]; David W. Thomas[†1]; Elaine L. Ferguson[†1]

10

11 [1]Advanced Therapies Group, Oral and Biomedical Sciences, School of Dentistry, College of

12 Biomedical and Life Sciences, Cardiff University, Heath Park, Cardiff, UK. [2]Department of

13 Pharmaceutical, Chemical and Environmental Sciences, Faculty of Engineering and Science,

14 University of Greenwich, Medway Campus, Central Avenue, Chatham Maritime, UK.

15 [3]Institut Laue-Langevin, DS/LSS group, 6 rue Jules Horowitz, 38042 Grenoble Cedex 9,

16 France. [4] Physical Organic Chemistry Centre, School of Chemistry, Cardiff University, Cardiff,

17 UK. [5]School of Biochemistry, Biomedical Sciences Building, University Walk, Clifton, BS8

18 1TD, UK. [6]Centre for NanoHealth, Systems and Process Engineering Centre, College of

19 Engineering, Swansea University, Swansea, UK. [7]AlgiPharma AS, Sandvika, Norway.

20 *Corresponding author (email: PritchardMF@cardiff.ac.uk). †Joint senior authors.

21

22

23

24

Concerns about acquisition of antibiotic resistance have led to increasing demand for new antimicrobial therapies. OligoG CF-5/20 is an alginate oligosaccharide previously shown to have antimicrobial and antibiotic potentiating activity. We investigated the structural modification of the bacterial cell wall by OligoG CF-5/20 and its effect on membrane permeability. Binding of OligoG CF-5/20 to the bacterial cell surface was demonstrated in Gram-negative bacteria. Permeability assays revealed that OligoG CF-5/20 had virtually no membrane-perturbing effects. Lipopolysaccharide (LPS) surface charge and aggregation were unaltered in the presence of OligoG CF-5/20. Small angle neutron scattering and circular dichroism spectroscopy showed no substantial change to the structure of LPS in the presence of OligoG CF-5/20, however, isothermal titration calorimetry demonstrated a weak calcium-mediated interaction. Metabolomic analysis confirmed no change in cellular metabolic response to a range of osmolytes when treated with OligoG CF-5/20. This data shows that, although weak interactions occur between LPS and OligoG CF-5/20 in the presence of calcium, the antimicrobial effects of OligoG CF-5/20 are not related to the induction of structural alterations in the LPS or cell permeability. These results suggest a novel mechanism of action that may avoid the common route in acquisition of resistance via LPS structural modification.

44 **Introduction**

45 Multi-drug resistant (MDR) bacteria represent a major global health challenge with soaring
46 morbidity and mortality [1]. Furthermore, as the acquisition of resistance now supersedes the
47 rate of development of new antibiotics, the need for novel antimicrobial therapies is urgent
48 [2]. OligoG CF-5/20 is a low molecular weight (Mn 3,200 g/mol) alginate derived from the stem
49 of the seaweed *Laminaria hyperborea* [3]. OligoG CF-5/20 potentiates the effect of
50 conventional antimicrobials against a range of bacteria [3] and fungi [4], and disrupts biofilm
51 formation of MDR pathogens both *in vitro* and *in vivo* [5]. However, the mechanism by which
52 OligoG CF-5/20 exerts its antimicrobial effects is still unclear. OligoG CF-5/20 has been
53 proven safe for human clinical use and is currently in Phase 2b clinical studies (NCT02157922;
54 NCT02453789) as an inhalation therapy for cystic fibrosis (CF) patients.

55 CF is an autosomal recessive disorder causing an imbalance in ion exchange across the
56 respiratory airway [6], leading to thick mucus stasis, which is ultimately chronically colonised
57 by opportunistic pathogens, principally *Pseudomonas aeruginosa* [7]. CF patients are especially
58 at risk of harbouring MDR bacteria due to the presence of chronic lung infection confounded
59 by intense and frequent use of multiple antibiotics from childhood. Having previously
60 demonstrated that OligoG CF-5/20 treatment was effectively associated with disruption of
61 planktonic and biofilm growth of *P. aeruginosa* [3,8,9], and that this effect was independent of
62 an interaction with the *P. aeruginosa mexAB-oprM* efflux pump system [3], this study sought to
63 investigate whether OligoG CF-5/20 exerts its antibiotic potentiation effects (up to 512-fold)
64 via direct interaction with the bacterial cell.

65 Whilst many antimicrobials act on the biosynthetic pathways of growing cells, the
66 bacterial membrane represents an important target in the treatment of quiescent non-
67 replicating bacteria in recalcitrant infection such as in the CF lung [10]. A number of agents

68 have been developed that modulate changes in the bacterial membrane directly, via
69 alterations in $NADH_2$ and ATP synthase, and indirectly, via generation of lethal reactive
70 oxygen species and nitric oxide in the bacterial membrane. Membrane active antibiotics,
71 such as the polymyxins, including colistin (polymyxin E) and polymyxin B, and amphipathic
72 antimicrobial peptides, such as RTA3 [11], act synergistically with other drugs to enhance their
73 internalisation and access to intracellular targets [12].
74 OligoG CF-5/20 modifies the surface charge of *P. aeruginosa*, inducing cellular aggregation
75 and a reduction in bacterial motility [8]; changes which are associated with decreased
76 mechanical strength of the biofilm structure [9]. A combination effect of OligoG CF-5/20 and
77 the antimicrobial triclosan against the oral pathogens *Streptococcus mutans* (Gram-positive)
78 and *Porphyromonas gingivalis* (Gram-negative) led to a decrease in attachment to surfaces
79 such as titanium [13]. Following the reported interaction of OligoG CF-5/20 with both these
80 Gram-negative and Gram-positive pathogens, a greater understanding of the interaction of
81 the oligosaccharide with the cell wall was sought. Gram-positive bacteria have a single lipid
82 membrane surrounded by a 30–100 nm thick peptidoglycan/lipoteichoic acid cell wall [14],
83 which is tightly cross-linked by inter-peptide bridges and has a phosphoryl group located in
84 the substituent teichoic and teichuronic acid residues, and unsubstituted carboxylate groups
85 (Fig. 1a). In comparison, Gram-negative bacteria have a very thin, loosely cross-linked
86 peptidoglycan, which is sequestered within the periplasmic space, between the inner and outer lipid
87 membranes. Phosphoryl and 2-keto-3-deoxyoctonate carboxylated groups of lipopolysaccharide
88 (LPS) are found in the outer leaflet of the outer membrane (Fig. 1b) [15]. Cell surface oligosaccharides
89 such as the hydrophilic *O*-antigen component of LPS in Gram-negative bacteria [16] also play a role in
90 facilitating biofilm attachment. The highly polyanionic nature of LPS maintains the integrity of the
91 outer membrane which is linked electrostatically by divalent cations such as Ca^{2+} [17]. The outer

membrane of Gram-negative bacteria is selectively resistant to noxious agents due to its effective permeability barrier function (enabling hydrophobic drugs to diffuse across the lipid bilayer, whilst small hydrophilic drugs use the porins to gain access to the cell). Both Gram-positive and Gram-negative bacteria have an overall negative electrostatic surface charge.

Here we present a range of nanoscale techniques to analyse the interaction of OligoG CF-5/20 with components of the bacterial cell wall and membrane permeability, in particular to *P. aeruginosa*. Detailed nanoscale analysis of the interaction of drugs with the bacterial cell can be used to enhance our understanding of the mechanism of action involved in antimicrobial therapy [18]. Atomic force microscopy (AFM) is fast becoming a common tool for analysing nanostructures [19] and has been used to study the effect of antimicrobial agents on planktonic cells [8,20,21] and bacterial biofilms [22,23] as well as a range of MDR Gram-negative organisms [24,25]. Cellular surface charge can be analysed using electrophoretic light scattering (ELS), now a standard method for measuring the zeta potential [26]. ELS is often used to explore mechanisms of bacterial adhesion and aggregation to biophysical host tissues and biomaterial substrates [27-29]. Small-angle neutron scattering (SANS) has previously been used to characterise the shape and interaction of bio-macromolecules such as antibiotics and polymers with key bacterial cell wall components, such as LPS [30]. Circular dichroism (CD) spectroscopy has been extensively used to characterise antimicrobial peptides [31] and analyse their interaction with the bacterial cell wall [32,33]. Here CD was used to monitor whether LPS interacts with OligoG CF-5/20 via its carboxyl groups that show intense Cotton effects near 200 and 215 nm [34]. Isothermal titration calorimetry has also previously been employed to elucidate the mechanisms by which novel antimicrobials interact with the cell surface target, LPS [35,36].

Results

116 **Comparison of bacterial cell wall and the effect of OligoG CF-5/20.** AFM images of Gram-
117 positive *S. mutans* and Gram-negative *P. aeruginosa* treated with OligoG CF-5/20 (7 and 5
118 mg/ml respectively), showed cellular aggregation, which was not evident in the untreated
119 bacteria (Fig. 1c). OligoG CF-5/20 appeared to surround the cell walls of *P. aeruginosa*
120 following a centrifugation step, prior to imaging. However, while Gram-positive *S. mutans*
121 demonstrated cellular clumping, OligoG CF-5/20 was not visible around the cell surface at the
122 nanoscale level upon exposure to centrifugation, when compared to *P. aeruginosa* (Fig. 1d).
123

124 **Effect of OligoG CF-5/20 on cell permeability.** Having demonstrated that OligoG CF-5/20 causes
125 cellular aggregation in Gram-negative bacteria, with OligoG CF-5/20 surrounding the cell walls, the
126 ability of the alginate to permeabilise both simulated (liposomes) and real cell membranes, with
127 propidium iodide (PI), nitrocefin (NFN) and 1-N-phenylnaphthylamine (NPN), was studied using
128 conventional permeability assays. Initial studies using carboxyfluorescein-loaded unilamellar
129 liposomes showed that, unlike RTA3 under these conditions, an amphipathic antimicrobial peptide,
130 OligoG CF-5/20 had virtually no membrane perturbing effects (Fig. 2a), although it did produce a
131 slight dose-dependent increase in release of trapped dye (Fig. 2b). Similar results were obtained in
132 vesicles composed of PC:PG at a ratio of 50:50 (data not shown).
133 Correspondingly, in an *in vitro* model of membrane permeabilisation in *P. aeruginosa* PAO1,
134 neither PI (Fig. 2c) nor NFN (Fig. 2d) were able to enter the cytoplasm and periplasmic space,
135 respectively, in the presence of OligoG CF-5/20. As OligoG CF-5/20 is able to bind Ca^{2+} we also
136 compared its effect to the chelating agent, ethylendiaminetetraacetic acid (EDTA), a chelator which
137 effectively permeabilises the bacterial outer membrane of PAO1, allowing internalisation of both the
138 dyes. In a final evaluation of the ability of OligoG CF-5/20 to enhance cell permeability,
139 internalisation of NPN dye by three *P. aeruginosa* strains was assessed. As seen in the other assays,

140 OligoG CF-5/20 (up to 20 mg/ml) did not promote partitioning of NPN into bacterial cell membranes,
141 which was clearly evident in the presence of the positive control, polymyxin B (Fig. 2e).

142

143 **Effect of OligoG CF-5/20 under various osmolyte conditions.** PAO1 (48 h) showed no changes in
144 growth in response to ionic/osmotic stress in the presence of OligoG CF-5/20 (20-60 mg/ml) under
145 all conditions tested, including 4% (w/v) urea (Fig. 3a) and 20 mM sodium benzoate pH 5.2 (Fig. 3b).

146

147 **Surface charge and aggregation of LPS in the presence of OligoG CF-5/20.** Having
148 eliminated the possibility of cell permeabilising effects, the direct interaction of OligoG CF-
149 5/20 with LPS was studied. First, LPS aggregate formation with OligoG CF-5/20 (or colistin
150 sulphate as a positive control) was studied by measuring change in turbidity over time.
151 Turbidity remained unaltered in the presence of OligoG CF-5/20 (up to 20 mg/ml), although
152 significant differences in turbidity were observed with the positive control, colistin sulphate,
153 which rapidly formed aggregates with LPS (Fig. 3c). Surface charge (zeta potential) of
154 pseudomonal LPS alone became slightly less negative as the pH increased from pH5 to pH7
155 and pH9 (-40.4 mV, -36.0 mV and -36.3 mV, respectively; Fig. 3d) with only a small overall
156 change in charge over this pH range (4.1 mV). In contrast, the zeta potential of OligoG CF-
157 5/20 alone showed a greater change in charge (11.4 mV) over the pH range tested, being
158 significantly less negative at pH 5 compared to pH 7 and 9 (-28.6 mV, -41.7 mV and -40.0 mV,
159 respectively; $p<0.05$). However, when OligoG CF-5/20 and LPS were combined, there was no
160 pH dependent change in surface charge interaction when compared to LPS alone.
161 **Structural interactions of OligoG CF-5/20 with LPS.** SANS experiments of LPS showed
162 significant scattering intensity I(Q) as a function of the wave-vector, Q, which varied subtly at

163 low Q as a function of ionic strength (Fig. 4a) but was largely unaltered by pH (see
164 Supplementary Fig. S1 online). Pre-incubation of LPS with OligoG CF-5/20 had no effect on
165 scattering intensity. However, when LPS was pre-incubated with a positive control, colistin
166 sulphate, a pronounced increase in scattering intensity at low Q was apparent, indicating
167 larger structures. Additionally, two peaks appeared at Q = 0.06 and 0.12 $Å^{-1}$, demonstrating a
168 regular structure of stacked interfaces (Fig. 4b). The most striking observation from the SANS
169 experiment, is that the scattering does not change with ionic strength or the addition of
170 OligoG CF-5/20. Indeed, when analysing the data in terms of a mixture of vesicles and
171 micelles, not surprisingly, the parameters required to fit the data were also largely constant.
172 The balance of the vesicular to micellar components was also invariant with both variables.
173 Noteworthy is the comparison of the radius in the micellar term (22 Å), presumably
174 corresponding to the extended length of the LPS molecule, *versus* the thickness of the
175 vesicular lamellae, 46 Å, which one would expect to be double the extended length.
176 CD spectra recorded under similar conditions showed no apparent conformational
177 changes that could indicate a specific LPS:OligoG CF-5/20 interaction. The spectra resulting
178 after mixing simply corresponded to the addition of the individual signals (Fig. 4c, d). This
179 was also found when varying the OligoG CF-5/20 concentration between 2 to 20 mg/ml (data
180 not shown). An ionic interaction of LPS with the carboxylates of OligoG CF-5/20 would be
181 expected to reduce the CD amplitude at ~215 nm and could induce a red-shift of the signal,
182 as observed for the interaction with calcium ions [37].
183 The SANS data also showed that Ca^{2+} at 5 and 10 mM had no effect on the LPS structure over
184 the length scale probed (Fig. 5a). The raw data follows a rather less curved form, with just a very
185 weak oscillation. The best fit here was found to be a given by the simple unilamellar vesicle with a
186 radius slightly larger than the previous case, but with a similar thickness, at least within experimental

187 error, *i.e.* there was no clear evidence of coexisiting smaller micelles. The key parameters for all
188 SANS experiments are presented in Table 1. Also, CD spectra for LPS/OligoG CF-5/20 interactions
189 measured with and without 5 mM Ca^{2+} at pH 5 and pH 7 showed no significant differences (Fig. 5b).
190
191 **Biomolecular interactions of OligoG CF-5/20 and LPS.** Initially, ITC was employed to record
192 the heat effects of OligoG CF-5/20 (20 mg/ml, ~6.25 mM) dilutions. The dilution heat effects
193 of OligoG CF-5/20 in the presence of 1 mM EDTA showed only a limited decrease, suggesting
194 that the aggregation state of OligoG CF-5/20 did not change with increasing concentration.
195 In the presence of 1 mM Ca^{2+}, however, the dilution heat effects were not constant and
196 followed the typical pattern for self-aggregating compounds [38], which was strongly
197 suggestive of OligoG CF-5/20 aggregation in the presence of added Ca^{2+}. (Data obtained in
198 the presence of 1 mM $CaCl_2$ were comparable to titrations in the presence of 1 mM EDTA and
199 2 mM $CaCl_2$, see Supplementary Fig. S2 online).
200 Further studies were conducted to determine the interaction between OligoG CF-5/20 and
201 LPS, both in the presence of 1 mM EDTA or $CaCl_2$ and when combining 1 mM EDTA and 2 mM
202 $CaCl_2$. In the presence of EDTA alone, (i.e. in the absence of free Ca^{2+}) the heat effects for
203 injection of OligoG CF-5/20 into LPS did not deviate significantly from the combined heat
204 effects for the reference dilution experiments (Fig. 6a). This observation suggested that in
205 the absence of free Ca^{2+}, OligoG CF-5/20 and LPS do not interact at the concentrations used
206 in these experiments. Contrastingly, in the presence of 1 mM added $CaCl_2$, (or 1 mM EDTA
207 and 2 mM $CaCl_2$), the heat effects observed for injection of OligoG CF-5/20 into LPS were
208 markedly different from the combined heat effects for the reference dilution experiments. In
209 particular, whilst de-aggregation of OligoG CF-5/20 upon dilution was exothermic (*vide*
210 *supra*), interaction of OligoG CF-5/20 with LPS was endothermic, strongly suggesting that

211 OligoG CF-5/20 and LPS interact in the presence of calcium (Fig. 6b). The lack of a sigmoidal
212 shape to the enthalpogram suggested that the interaction was weak [39].
213
214 **Discussion**
215 OligoG CF-5/20 is a new antimicrobial therapy, demonstrating promising results across the
216 microbial kingdom in both eubacteria and yeasts. Effective synergistic enhancement of
217 current antimicrobials has previously been demonstrated in both Gram-positive [13] and Gram-
218 negative bacteria [3]. This study focused on the nanoscale interaction of OligoG CF-5/20 with
219 the Gram-negative cell surface, following strong, irreversible binding to the cell wall after
220 centrifugation. OligoG CF-5/20 has previously been shown to remain bound to the
221 pseudomonal cell surface, leading to cellular aggregation, even after exposure to
222 hydrodynamic shear [8].
223 Structural analysis of pseudomonal biofilms has previously indicated that OligoG CF-5/20
224 treatment was associated with increased water channels as demonstrated by scanning
225 electron and confocal laser scanning microscopy studies [3] and a decrease in biofilm strength
226 as shown by rheological analysis and AFM [9]. Clear differences were seen at the nanoscale
227 level, showing significantly greater surface interaction of OligoG CF-5/20 with the Gram-
228 negative cell wall of *P. aeruginosa,* which remained attached to the *P. aeruginosa* cell wall,
229 and resisted hydrodynamic shear [8]. A previous study quantified the alteration in PAO1
230 surface charge and aggregation using electrophoretic and dynamic light scattering, and
231 confirmed the irreversible binding between OligoG CF-5/20 and the cell surface [8]. No change
232 in surface charge was seen with the Gram-positive *S. mutans* when treated with OligoG CF-
233 5/20 following hydrodynamic shear (Supplementary Fig. S3 online). The presence of a dense
234 layer of LPS is unique to Gram-negative bacteria and provides an effective (although

235 selective) permeability barrier [40]. We hypothesised that OligoG CF-5/20 may directly interact
236 with LPS to reduce biofilm formation and further experiments were conducted solely in
237 Gram-negative *P. aeruginosa* strains.

238 Permeabilisation studies in *P. aeruginosa* demonstrated that the cellular membrane
239 changes induced by membrane-active agents, EDTA, and polymyxin B and the synthetic
240 peptide RTA3, were virtually absent in the presence of OligoG CF-5/20 (Fig. 2). Similarly,
241 metabolomic-profiling studies demonstrated that bacterial growth with OligoG CF-5/20 was
242 unaffected by changes in osmotic/ionic conditions (Fig. 3a, b). The lack of permeabilisation
243 was supported by growth assays that showed only bacteriostatic activity with OligoG CF-5/20
244 [3]. Nevertheless, this could be advantageous as the development of many membrane-active
245 antimicrobial agents has been hampered by formulation difficulties and non-specific
246 permeabilisation/toxicity concerns [41]. The putative membrane effect with OligoG CF-5/20 is
247 supported by the absence of resistance to the drug during prolonged serial passage [3].

248 Previous force-curve measurements on *P. aeruginosa* PAO1 biofilms showed a decrease in
249 Young's modulus when treated with OligoG CF-5/20 (20-100 mg/ml) [9], which correlated with
250 an alteration (3.1-6.0 mV decrease) in surface charge [8]. However, these results were not
251 reflected in the LPS ELS analysis in this study (Fig. 3d). Conversely, previous studies have
252 noted that ELS and AFM analysis for LPS may not always correlate, as bacterial adhesion can
253 vary depending on LPS chain length [42].

254 SANS and CD experiments were employed to gain a greater understanding of the
255 interaction of OligoG CF-5/20 with Gram-negative cell wall components at the nanoscale.
256 SANS has previously been used to analyse the structure of LPS and its derivatives,
257 highlighting the different chemotypes of LPS (rough and smooth) and the importance of
258 temperature control [43-45]. In these studies, colistin was used as a positive control due to its

259 known ability to bind and neutralise bacterial LPS [46] displacing cell wall-stabilising divalent
260 cations in the outer membrane [47]. Previous studies have investigated the direct interaction
261 of colistin with LPS from *Escherichia coli* using turbidity, CD and SANS experiments [30].
262 Pseudomonal LPS aggregates demonstrated a high scattering intensity, $I(Q)$ as a function of
263 the wave-vector, Q, which was in line with the size, shape and distribution of *E. coli* LPS
264 observed previously [30]. These studies, along with others [48], have demonstrated that at
265 neutral pH, LPS forms structures that are hundreds of nm in size but with a lamellar
266 organization and bilayer thickness of ~5 nm. Similarly, the emergence of two peaks when LPS
267 was treated with colistin, was accompanied by a pronounced increase in scattering intensity
268 at low Q, as seen with *E. coli* LPS and colistin [30]. The conformation of the LPS was unaltered
269 by OligoG CF-5/20 at all pHs and salt concentrations tested (Fig. 4a, b), which are comparable
270 to those previously reported in PAO1 zeta potential analysis [8]. Similar to the current study,
271 CD spectra of LPS-colistin mixtures showed no indication of conformational changes, but only
272 changes that could be interpreted as simple additive effects (Fig. 4c, d).
273 Salt concentration and pH have a fundamental effect on bacterial surface charge, and
274 these parameters are altered in CF patients during an exacerbation and when in remission.
275 Several studies have shown a broad variation of acidity in the lung environment of a CF
276 patient (pH 5-6) which is lowered during an exacerbation, while normal lung fluid pH is ~7
277 [49,50]. Similarly, the chloride concentration of CF lung fluid is abnormally high, due to defective
278 chloride channels and/or chronic lung infection and inflammation with the chloride
279 concentration of tracheal and bronchial airway surface fluid increasing from 85 ± 54 mM in
280 healthy individuals to 129 ± 79 mM in CF patients [51]. Encouragingly, these studies
281 demonstrate that OligoG CF-5/20 did not cause any conformational changes in LPS at
282 physiological pH and salt concentrations.

283 The discovery that the antimicrobial activity of OligoG CF-5/20 does not depend on cell
284 permeabilisation is promising, since this is the type of mechanism of action that is commonly
285 found to be the cause of antibiotic resistance [52]. Colistin is increasingly being used for the
286 treatment of MDR Gram-negative bacterial infections [53] and is the most commonly inhaled
287 antibiotic treatment in CF [54]. The recent emergence of colistin resistance is of major concern
288 [55] and is linked to LPS modification [56] possibly as a result of complete loss of LPS in strains
289 such as *Acinetobacter baumannii* [57]. LPS modification mediated by the *pmr* operon is also
290 known to enhance colistin resistance [58]. Recently, OligoG CF-5/20 has been shown to
291 potentiate the effect of colistin against MDR pseudomonal pathogens, leading to a 128-fold
292 reduction in the Minimum Biofilm Eradication Concentration value [5].
293 A significant alteration in divalent cation levels has been reported in the CF lung (102 mg/l Ca^{2+})
294 compared to 45 mg/l in a healthy control [59]. The effect of divalent metal ions in maintaining LPS
295 structure has been well documented in the literature, with their depletion found to lead to a distinct
296 outer membrane structure with an exposed peptidoglycan surface layer, and increased cell
297 permeability [40]. Colistin is believed to electrostatically bind to the anionic phosphate groups on the
298 LPS lipid A core, leading to displacement of the divalent cations which bridge the lipid A molecules
299 and maintain cell wall integrity [47]. Previous *in vivo* biofilm models of MDR infection, have
300 demonstrated a dramatic reduction in biofilm growth (>3-log fold) when colistin treatment was
301 combined with OligoG CF-5/20 administered intra-tracheally [5].
302 Gram-negative bacteria do not reflect membrane perturbation following binding. Instead we
303 hypothesise that the anti-biofilm effects of OligoG CF-5/20 are mediated via interaction with the
304 bacterial matrix of extracellular polysaccharide substance (EPS), removing this barrier and allowing
305 more effective interaction of colistin with the bacterial cell wall. This mechanism of action, by EPS
306 disruption, may be promising in the treatment of MDR biofilm infections [60].

307 Due to its overall negative charge, OligoG CF-5/20 did not self-aggregate in the absence of
308 free Ca^{2+}. However, Ca^{2+}-induced self-aggregation can overcome the electrostatic repulsion
309 between individual molecules, via the formation of salt bridges. In fact, previous calorimetric
310 studies have shown similar Ca^{2+}-mediated aggregation of alginates via so-called 'egg-box'
311 dimers[61]. Unsurprisingly, the interaction between OligoG CF-5/20 and LPS was also found to
312 be mediated by Ca^{2+}, but the interaction was not sufficiently strong enough to allow analysis
313 in terms of a simple binding model (stoichiometry and affinity). The ITC studies concluding
314 that only a weak (Ca^{2+} dependent) interaction between OligoG CF-5/20 and LPS occurred,
315 alongside the physical analysis (ITC/SANS/CD spectroscopy), all suggested that OligoG CF-
316 5/20 did not significantly alter the structure of LPS. These interactions may, in part, be
317 reflected in the bacterial aggregation observed in AFM.
318 In summary, OligoG CF-5/20 induced cellular aggregation of both *S. mutans* and *P.*
319 *aeruginosa*, however, irreversible surface interaction of OligoG CF-5/20 was demonstrated
320 with the Gram-negative cell. No increase in permeability of the membrane was detected
321 when treated with OligoG CF-5/20. OligoG CF-5/20 also did not induce surface charge
322 alterations of the LPS component of the outer membrane, nor did it neutralise or cause
323 aggregation of LPS itself. Subtle changes in LPS conformation were recorded in solution
324 following an increase in salt concentration, however pH had no apparent effect. CD spectra
325 for LPS remained unaltered by OligoG CF-5/20, as did the presence of Ca^{2+}. ITC, however,
326 showed a weak Ca^{2+} mediated interaction between OligoG CF-5/20 and LPS. Studies are
327 ongoing to determine the molecular mechanism of action of the antimicrobial properties of
328 OligoG CF-5/20. It is hoped that defining its mode of action will help with the development
329 of future applications for this antimicrobial agent, to address the developmental need for
330 new antimicrobial therapies.

331

332 **Materials and Methods**

333 **Materials.** OligoG CF-5/20 was synthesised as previously described [3]. Materials were obtained from

334 the following companies: deuterium oxide (D_2O; with 99.9% isotopic purity), LPS (from *Pseudomonas*

335 *aeruginosa* 10), Triton X-100, carboxyfluorescein (Cbfl), colistin sulphate, polymyxin B, Tris HCl,

336 propidium iodide (PI), 1-*N*-phenylnapthylamine (NPN), ethylenediaminetetraacetic acid (EDTA),

337 sodium fluoride (Sigma-Aldrich, Gillingham, U.K.); sodium chloride (NaCl), calcium chloride (CaCl),

338 hydrochloric acid, sodium hydroxide, acetone (Fisher Scientific, Loughborough, U.K.); phosphate

339 buffered saline (PBS) tablets, tryptic soy broth (TSB), Mueller-Hinton (MH) broth, (Oxoid,

340 Basingstoke, U.K.); nitrocefin, (Calbiochem, Darmstadt, Germany); and egg phosphatidylcholine (PC),

341 phosphatidylglycerol (PG), (Lipid Products, Nutfield, UK).

342

343 **Bacteria, Media and Culture Conditions.** *Streptococcus mutans* DSM 20523 (ATCC 25175) and

344 *Pseudomonas aeruginosa* strains PAO1, V2 (MDR[3]) and NH57388A (mucoid variant) were grown on

345 blood agar plates or in TSB overnight at 37°C.

346

347 **Atomic Force Microscopy Imaging.** Bacterial cultures of *S. mutans* DSM 20523 (72 h) and *P.*

348 *aeruginosa* (PAO1; 24 h) were grown in TSB at 37°C. The overnight cultures were washed twice

349 (5,500 *g*, 3 mins) in dH_2O and the bacteria were then incubated in 5-7 mg/ml OligoG CF-5/20 for 20

350 mins. Excess OligoG CF-5/20 was removed (2,500 *g,* 6 mins) before resuspending the bacterial cells

351 in dH_2O and drying on 0.01% poly-L-lysine coated mica plates for imaging. A Dimension 3100 AFM

352 (Bruker) was used, using tapping mode operation in air (0.8 Hz scan speed).

353

354 **Membrane permeability studies.**

355 ***Release of carboxyfluorescein dye from a vesicular model of the bacterial membrane.*** This model,
356 mimicking the Gram-negative bacterial inner membrane, was used to study membrane interactions
357 with OligoG CF-5/20. Small unilamellar liposomes (100 nm) containing carboxyfluorescein (Cbfl; 50
358 mM) were prepared from egg phospholipids employing the freeze/thaw pressure-extrusion
359 method[11,62] using egg phosphatidylcholine:phosphatidylglycerol at a ratio of 80:20 or 50:50 to mimic
360 the Gram-negative bacterial inner membrane. Cbfl solutions were made by dissolving in 10 mM Tris
361 and adding NaOH to bring the pH to 7.4. Dried phospholipids were hydrated in Cbfl-containing Tris,
362 pH 7.4, freeze-thawing 3 times to support the production of large multilamellar vesicles at a lipid
363 concentration of 10 mg/ml, and then extruding 10 times through two 100 nm pore membranes. The
364 resulting Cbfl-loaded 100 nm small unilamellar vesicles were separated from external Cbfl by passing
365 down a Sephadex G-15 gel filtration column equilibrated with 10 mM Tris, pH 7.4 containing 107
366 mM NaCl to balance osmotically the internal Cbfl. Release of entrapped Cbfl in the presence of
367 OligoG CF-5/20 (20, 60, 100 mg/ml) was measured in 10 mM Tris-HCl, 107 mM NaCl (pH 7.4) buffer
368 by fluorescence with λ_{ex} = 490 nm and λ_{em} = 520 nm over time (5 mins). RTA3 [11] (0.5 µM) and Tris
369 buffer alone were used as positive and negative controls, respectively.
370
371 ***Determination of membrane permeabilisation by nitrocefin and propidium iodide uptake of cells.***
372 Membrane permeabilisation of PAO1 was quantified by measuring cellular uptake of nitrocefin (a
373 chromogenic β-lactamase substrate) [63] or propidium iodide (PI) [64]. Cells were grown overnight in
374 TSB, then diluted in PBS (pH 7.4) to an OD_{625} of 0.5. Cells were then washed twice by centrifugation
375 at 3,500 *g* for 10 min at 25°C to form a pellet, before being resuspended in PBS.
376 For the nitrocefin assay, OligoG CF-5/20 (0, 20, 60, 100 mg/ml) or EDTA (10 mM) dissolved in PBS
377 (180 µl) were added to the wells of a microtitre plate containing bacterial suspension (10 µl). The
378 plate was sealed with parafilm, incubated at 37°C for 3 h and centrifuged at 12,000 *g* for 10 min.

379 The supernatant (95 µl) of each well was removed and transferred into the wells of a clean
380 microtitre plate containing nitrocefin (0.5 mg/ml in 5% v/v DMSO, 5 µl). Plates were incubated in
381 the dark at 37°C for 30 min before measuring the absorbance on a FLUOstar OPTIMA plate reader
382 (BMG LABTEC) at 486 nm (n=3).
383 For the PI assay, OligoG CF-5/20 (0, 20, 60, 100 mg/ml) or EDTA (10 mM) dissolved in PBS (140 µl)
384 were added to the wells of a black microtitre plate containing bacterial suspension (10 µl) and PI
385 solution (1.5 mM in PBS, 50 µl). Plates were incubated in the dark at 37°C for 15 min before
386 measuring fluorescence (λ_{ex} = 480 nm, λ_{em} = 612 nm). Fluorescence intensity was calculated by
387 subtracting the baseline fluorescence of control cells (PBS only) from the total fluorescence of
388 treated cells (n=3).
389
390 ***1-N-phenylnaphthylamine (NPN) dye assay.*** Outer membrane permeabilisation of *P.*
391 *aeruginosa* was quantified by measuring uptake of 1-*N*-phenylnapthylamine (NPN) dye into
392 the bacterial cytoplasmic membrane [65]. Cells were grown overnight in TSB then diluted in
393 PBS, pH 7.4, to an OD_{625} of 0.5. Cells were washed twice by centrifugation at 4,000 rpm for
394 10 min at 25°C and resuspended in PBS. Bacterial suspension (100 µl) was added to the wells
395 of a black 96-well plate and mixed with freshly prepared NPN solution (40 µM in 8% v/v
396 acetone; 50 µl) and left to equilibrate at room temperature for 30 min. Solutions (50 µl) of
397 OligoG CF-5/20 (0, 2, 20 mg/ml) or polymyxin B (10 µg/ml) were added to the wells and
398 fluorescence was read immediately using the fluorescent plate reader (λ_{ex} = 350 nm, λ_{em} =
399 410 nm). Dye uptake was calculated by subtracting the baseline fluorescence of free NPN
400 from the total fluorescence of treated cells (n=12).
401

402 **Effect of OligoG CF-5/20 under various osmolyte conditions.** Metabolomic studies were employed
403 to phenotypically screen for the effect of osmolytes on *P. aeruginosa* PAO1 using an osmotic/ionic
404 response assay panel from BIOLOG (Haywood, CA, USA), a 96 well-plate containing different
405 osmolytic conditions [66]. PAO1 was grown overnight on 5% Blood agar at 37°C. OligoG CF-5/20 (20-
406 60 mg/ml) was dissolved in Innoculating Fluid (IF) 10 (BIOLOG) and incubated at 37°C for 20-30 min
407 on a roller mixer until dissolved. The remaining ingredients (inoculating fluid base, dye mix, cells and
408 water) were added according to the manufacturers' instructions prior to loading onto the BIOLOG
409 PM09 plate (100 µl/well). OligoG CF-5/20 and PAO1 only controls were also included. Plates were
410 incubated in an Omnilog incubator at 37°C for 120 h. As there was no change of activity after this
411 time, results were taken at 48 h. Metabolic activity was analysed colorimetrically by measuring
412 reduction of tetrazolium dye to insoluble formazan (purple colour) by cell respiration [67] (n=2). An
413 OligoG CF-5/20 only control (≥ 60 mg/ml) was included to confirm that no colometric changes in the
414 absence of PAO1 occurred.
415
416 **Electrophoretic light scattering (zeta potential) measurements.** The surface charge of
417 pseudomonal LPS (10 mg/ml) in the absence and presence of OligoG CF-5/20 (2 mg/ml) was
418 determined using a Zetasizer Nano ZS (Malvern Instruments) with disposable capillary cells (DTS1061
419 Malvern Instruments) in 0.01 M NaCl, pH 5, 7 and 9, at 25°C (n=10).
420
421 **Turbidity assay.** A turbidimetric assay was used to measure the binding of OligoG CF-5/20 to
422 LPS resulting from the precipitation of aggregates and increased turbidity. LPS was dissolved
423 in pre-warmed PBS (10 mg/ml, 37°C, pH 7.4) containing OligoG CF-5/20 (2 and 20 mg/ml) and
424 200 µl were added to the wells of a 96-well microtitre plate. Control samples contained only
425 LPS dissolved in PBS. Plates were incubated at 37°C throughout the experiment and

426 absorbance was read at 620 nm at time-points over 2 h. Samples were assayed in triplicate
427 and means calculated.
428
429 **Small angle neutron scattering (SANS).** SANS experiments were performed either on the D11
430 diffractometer at the steady-state reactor source ILL, Grenoble or on SANS2d at the spallation
431 source at ISIS, Oxfordshire. For D11, measurements were performed at a constant neutron
432 wavelength (λ) of 6 Å and sample-detector distances of 1.2 m and 8 m to cover a Q range between
433 0.008 and 0.5 $Å^{-1}$, whereas for SANS2D, neutron wavelengths spanning 2-14 Å were used to access a
434 Q range 0.02 to 3 $Å^{-1}$. In both cases, the samples were contained in 2 mm path-length, UV-
435 spectrophotometer grade quartz cuvettes (Hellma, U.K.) and mounted in aluminium holders on top
436 of an enclosed, computer-controlled, sample chamber. Sample volumes were around 0.4 cm^3. All
437 experiments were conducted at 37°C ± 0.2°C. Experimental measuring times were approximately 20
438 min.
439 To assess the salt- and pH-dependent solution conformation of OligoG CF-5/20, the
440 polymer was dissolved (20 mg/ml) in D_2O containing 0.001 M, 0.01 M or 0.1 M NaCl at pH 5,
441 7, or 9. To characterise the OligoG CF-5/20-LPS interaction, LPS (10 mg/ml) was incubated in
442 the absence and presence of OligoG CF-5/20 (2, 20 mg/ml) in D_2O containing 0.001 M, 0.01
443 M or 0.1 M NaCl at pH 5, 7, or 9 for 3 h at 37°C prior to analysis by SANS. Where relevant,
444 calcium chloride was also included to the stated concentration.
445 All scattering data were (a) normalised for the sample transmission, (b) background
446 corrected using a quartz cell filled with D_2O, and (c) corrected for the linearity and efficiency
447 of the detector response using the instrument specific software package.
448 The data without calcium were fitted to a model comprising a coexisting mixture of
449 unilamellar vesicular and spherical micellar structures. However, when combined with

450 calcium, a vesicular structure model, looking at the absolute scattering intensities was

451 utilised[43].

452

453 **Circular dichroism spectroscopy.** CD was used to look at the interaction of LPS with OligoG CF-5/20.

454 Spectra were recorded on an Aviv 215 spectrophotometer (Aviv Biomedical Inc., Lakewood, NJ) using

455 0.01-cm quartz cuvettes. Samples were prepared by dilution from 25 mg/ml LPS and 50 mg/ml

456 OligoG CF-5/20 stock solutions into the desired buffers and incubated for 3 to 6 h at 37°C prior to

457 measurements. Spectra were recorded using a 1 nm bandwidth, 0.2 nm intervals with 3 s

458 accumulation time at 37°C with a dynode voltage less than 500 V. Buffer baselines recorded in the

459 same cell with the same parameters were subtracted. Mean residue weight ellipticities are reported

460 using 194 Da to represent the mass of the carbohydrate units.

461

462 **Isothermal Titration Calorimetry (ITC).** Calorimetric titrations were carried out at 37 °C on a

463 MicroCal PEAQ-ITC microcalorimeter (Malvern Instruments Ltd). The instrument was operated

464 applying a reference power of 10 µcal/s, in high feedback mode, stirring the sample cell contents at

465 750 rpm, with a pre-injection initial delay of 60 s. Freshly prepared solutions of LPS (10 mg/ml, ~0.5

466 mM) and OligoG CF-5/20 (20 mg/ml, ~6.25 mM) were loaded into the calorimeter sample cell and

467 injection syringe respectively, using the required buffers. Buffers employed in the experiment were

468 100 mM NaCl, 20 mM NaH_2PO_4 (+ NaOH adjusted to pH 7) ± the addition of 1 mM EDTA and/or $CaCl_2$

469 (1 mM final free Ca^{2+}). All experiments involved an initial injection of 0.4 µL in 0.8 s followed by 18

470 further injections of 2.0 µL in 4.0 s into the calorimeter sample cell. Injections were spaced by at

471 least 90 s to allow full recovery of the baseline. Raw data was treated using MicroCal PEAQ-ITC

472 Analysis Software (1.0.0.1259) to generate both integrated heat effects per injection (ΔQ) and molar

473 heat effects per injection (ΔH).

474

475 **Statistical analysis.** The significance of the data was assessed using one-way analysis of variance

476 (ANOVA) followed by Bonferroni's post hoc test. Statistical significance was set at $p < 0.05$.

477

478 **References**

479 1 Alanis, A. J. Resistance to antibiotics: Are we in the post-antibiotic era? *Arch. Med. Res.*
480 **36**, 697-705 (2005).
481 2 Laxminarayan, R. *et al.* Antibiotic resistance-the need for global solutions. *Lancet Infect.*
482 *Dis.* **13**, 1057-1098 (2013).
483 3 Khan, S. *et al.* Overcoming drug resistance with alginate oligosaccharides able to
484 potentiate the action of selected antibiotics. *Antimicrob. Agents Chemother.* **56**, 5134-
485 5141 (2012).
486 4 Tøndervik, A. *et al.* Alginate oligosaccharides inhibit fungal cell growth and potentiate
487 the activity of antifungals against *Candida* and *Aspergillus* spp. *Plos One* **9**,
488 10.1371/journal.pone.0112518d (2014).
489 5 Hengzhuang, W. *et al.* OligoG CF-5/20 Disruption of mucoid *Pseudomonas aeruginosa*
490 biofilm in a murine lung infection model. *Antimicrob. Agents Chemother.* **60**, 2620-2626
491 (2016).
492 6 Cohen, T. S. & Prince, A. Cystic fibrosis: a mucosal immunodeficiency syndrome. *Nat.*
493 *Med.* **18**, 509-519 (2012).
494 7 Folkesson, A. *et al.* Adaptation of *Pseudomonas aeruginosa* to the cystic fibrosis airway:
495 an evolutionary perspective. *Nat. Rev. Microbiol.* **10**, 841-851 (2012).
496 8 Powell, L. C. *et al.* A nanoscale characterization of the interaction of a novel alginate
497 oligomer with the cell surface and motility of *Pseudomonas aeruginosa*. *Am. J. Respir.*
498 *Cell Mol. Biol.* **50**, 483-492 (2014).
499 9 Powell, L. C. *et al.* The effect of alginate oligosaccharides on the mechanical properties
500 of Gram-negative biofilms. *Biofouling* **29**, 413-421 (2013).
501 10 Hurdle, J. G., O'Neill, A. J., Chopra, I. & Lee, R. E. Targeting bacterial membrane function:
502 an underexploited mechanism for treating persistent infections. *Nat. Rev. Microbiol.* **9**,
503 62-75 (2011).
504 11 Hawrani, A., Howe, R. A., Walsh, T. R. & Dempsey, C. E. Origin of low mammalian cell
505 toxicity in a class of highly active antimicrobial amphipathic helical peptides. *J. Biol.*
506 *Chem*. **283**, 18636-18645 (2008).
507 12 Delcour, A. H. Outer membrane permeability and antibiotic resistance. *BBA-Proteins*
508 *Proteomics* **1794**, 808-816 (2009).
509 13 Roberts, J. L. *et al.* An *in vitro* study of alginate oligomer therapies on oral biofilms. *J.*
510 *Dent* **41**, 892-899 (2013).
511 14 Silhavy, T. J., Kahne, D. & Walker, S. The bacterial cell envelope. *Cold Spring Harbor*
512 *Perspect.* **2**, doi:10.1101/cshperspect.a000414 (2010).
513 15 Wilson, W. W., Wade, M. M., Holman, S. C. & Champlin, F. R. Status of methods for
514 assessing bacterial cell surface charge properties based on zeta potential measurements.
515 *J. Microbiol. Methods* **43**, 153-164 (2001).

516 16 Kipnis, E., Sawa, T. & Wiener-Kronish, J. Targeting mechanisms of *Pseudomonas*
517 *aeruginosa* pathogenesis. *Med. Mal. Infect.* **36**, 78-91 (2006).
518 17 Vaara, M. Agents that increase the permeability of the outer-membrane. *Microbiol. Rev.*
519 **56**, 395-411 (1992).
520 18 Reviakine, I. & Brisson, A. Formation of supported phospholipid bilayers from
521 unilamellar vesicles investigated by atomic force microscopy. *Langmuir* **16**, 1806-1815
522 (2000).
523 19 Palmer, L. C. & Stupp, S. I. Molecular self-assembly into one-dimensional nanostructures.
524 *Accounts Chem. Res.* **41**, 1674-1684 (2008).
525 20 Kasas, S., Fellay, B. & Cargnello, R. Obervation of the action of penicillin on *Bacillus*
526 *subtilis* using atomic force microscopy- technique for the preparation of bacteria. *Surf.*
527 *Interface Anal.* **21**, 400-401 (1994).
528 21 Braga, P. C. & Ricci, D. Atomic force microscopy: Application to investigation of
529 *Escherichia coli* morphology before and after exposure to cefodizime. *Antimicrob.*
530 *Agents Chemother.* **42**, 18-22 (1998).
531 22 Bekir, K., Noumi, E., Abid, N. B. S. & Bakhrouf, A. Adhesive properties to materials used
532 in unit care by *Staphylococcus aureus* strains incubated in seawater microcosms. *J. Ind.*
533 *Eng. Chem.* **20**, 2447-2451 (2014).
534 23 Beech, I. B., Smith, J. R., Steele, A. A., Penegar, I. & Campbell, S. A. The use of atomic
535 force microscopy for studying interactions of bacterial biofilms with surfaces. *Colloid*
536 *Surf. B-Biointerfaces* **23**, 231-247 (2002).
537 24 Soon, R. L., Nation, R. L., Hartley, P. G., Larson, I. & Li, J. Atomic force microscopy
538 investigation of the morphology and topography of colistin-heteroresistant
539 *Acinetobacter baumannii* strains as a function of growth phase and in response to
540 colistin treatment. *Antimicrob. Agents Chemother.* **53**, 4979-4986 (2009).
541 25 Rossetto, G. *et al.* Atomic force microscopy evaluation of the effects of a novel
542 antimicrobial multimeric peptide on *Pseudomonas aeruginosa*. *Nanomed.-Nanotechnol.*
543 *Biol. Med.* **3**, 198-207 (2007).
544 26 Cowan, M. M., Vandermei, H. C., Stokroos, I. & Busscher, H. J. Heterogeneity of surfaces
545 of subgingival bacteria as detected by zeta potential measurements. *J. Dent. Res.* **71**,
546 1803-1806 (1992).
547 27 Alves, C. S. *et al. Escherichia coli* cell surface perturbation and disruption induced by
548 antimicrobial peptides BP100 and pepR. *J. Biol. Chem.* **285**, 27536-27544 (2010).
549 28 Roosjen, A., Busscher, H. J., Nordel, W. & van der Mei, H. C. Bacterial factors influencing
550 adhesion of *Pseudomonas aeruginosa* strains to a poly(ethylene oxide) brush.
551 *Microbiology-SGM* **152**, 2673-2682 (2006).
552 29 Shephard, J., McQuillan, A. J. & Bremer, P. J. Mechanisms of cation exchange by
553 *Pseudomonas aeruginosa* PAO1 and PAO1 wbpL, a strain with a truncated
554 lipopolysaccharide. *Appl. Environ. Microbiol.* **74**, 6980-6986 (2008).
555 30 Roberts, J. L. *et al. In vitro* evaluation of the interaction of dextrin-colistin conjugates
556 with bacterial lipopolysaccharide. *J. Med. Chem.* **59**, 647-654 (2016).
557 31 Wu, M. H. & Hancock, R. E. W. Interaction of the cyclic antimicrobial cationic peptide
558 bactenecin with the outer and cytoplasmic membrane. *J. Biol. Chem.* **274**, 29-35 (1999).
559 32 Turner, J., Cho, Y., Dinh, N. N., Waring, A. J. & Lehrer, R. I. Activities of LL-37, a cathelin-
560 associated antimicrobial peptide of human neutrophils. *Antimicrob. Agents Chemother.*
561 **42**, 2206-2214 (1998).

562 33 Falla, T. J., Karunaratne, D. N. & Hancock, R. E. W. Mode of action of the antimicrobial
563 peptide indolicidin. *J. Biol. Chem.* **271**, 19298-19303 (1996).
564 34 Liang, J. N., Stevens, E. S., Frangou, S. A., Morris, E. R. & Rees D. A. Cation-specific
565 vacuum ultraviolet circular dichroism behaviour of alginate solutions, gels and solid
566 films. *Int. J. Biol. Macromol.* **2**, 204-208 (1980).
567 35 Shang, D. J., Zhang, Q., Dong, W. B., Liang, H. & Bi, X. N. The effects of LPS on the activity
568 of Trp-containing antimicrobial peptides against Gram-negative bacteria and endotoxin
569 neutralization. *Acta Biomater.* **33**, 153-165 (2016).
570 36 McCaughey, L. C. *et al.* Discovery, characterization and *in vivo* activity of pyocin SD2, a
571 protein antibiotic from *Pseudomonas aeruginosa. Biolchem. J.* **473**, 2345-2358 (2016).
572 37 Grant, G. T., Morris, E. R., Rees, D. A., Smith, P. J. C. & Thom, D. Biological interactions
573 between polysaccharides and divalent cations: The egg-box model. *FEBS Lett.* **32**, 195-
574 198 (1973).
575 38 Buurma, N. J. & Haq, I. Advances in the analysis of isothermal titration calorimetry data
576 for ligand-DNA interactions. *Methods*. **42**, 162-172 (2007).
577 39 Turnbull, W. B. & Daranas, A. H. On the value of c: Can low affinity systems be studied by
578 isothermal titration calorimetry? *J. Am. Chem. Soc.* **125**, 14859-14866, (2003).
579 40 Amro, N. A. *et al.* High-resolution atomic force microscopy studies of the *Escherichia coli*
580 outer membrane: Structural basis for permeability. *Langmuir* **16**, 2789-2796 (2000).
581 41 Hancock, R. E. W. & Sahl, H. G. Antimicrobial and host-defense peptides as new anti-
582 infective therapeutic strategies. *Nat. Biotechnol.* **24**, 1551-1557 (2006).
583 42 Razatos, A., Ong, Y. L., Sharma, M. M. & Georgiou, G. Molecular determinants of
584 bacterial adhesion monitored by atomic force microscopy. *Proc. Natl. Acad. Sci. U.S.A.*
585 **95**, 11059-11064 (1998).
586 43 Bello, G. *et al.* Characterization of the aggregates formed by various bacterial
587 lipopolysaccharides in solution and upon interaction with antimicrobial peptides.
588 *Langmuir* **31**, 741-751 (2015).
589 44 D'Errico, G. *et al.* Mesoscopic and microstructural characterization of liposomes formed
590 by the lipooligosaccharide from *Salmonella minnesota* strain 595 (Re mutant). *Phys.*
591 *Chem. Chem. Phys.* **11**, 2314-2322 (2009).
592 45 D'Errico, G. *et al.* Characterization of liposomes formed by lipopolysaccharides from
593 *Burkholderia cenocepacia, Burkholderia multivorans* and *Agrobacterium tumefaciens*:
594 from the molecular structure to the aggregate architecture. *Phys. Chem. Chem. Phys.* **12**,
595 13574-13585 (2010).
596 46 Davies, B. & Cohen, J. Endotoxin removal devices for the treatment of sepsis and septic
597 shock. *Lancet Infect. Dis.* **11**, 65-71 (2011).
598 47 Velkov, T., Thompson, P. E., Nation, R. L. & Li, J. Structure-activity relationships of
599 polymyxin antibiotics. *J. Med. Chem.* **53**, 1898-1916 (2010).
600 48 Labischinski, H., Vorgel, E., Uebach, W., May, R. P. & Bradaczek, H. Architecture of
601 bacterial lipid A in solution. A small angle scattering study. *Eur. J. Biochem.* **190**, 359-363
602 (1990).
603 49 Tate, S., MacGregor, G., Davis, M., Innes, J. A. & Greening, A. P. Airways in cystic fibrosis
604 are acidified: detection by exhaled breath condensate. *Thorax* **57**, 926-929 (2002).
605 50 Newport, S., Amin, N. & Dozor, A. J. Exhaled breath condensate pH and ammonia in
606 cystic fibrosis and response to treatment of acute pulmonary exacerbations. *Pediatr.*
607 *Pulmonol.* **44**, 866-872 (2009).

608 51 Joris, L., Dab, I. & Quinton, P. M. Elemental composition of human airway surface fluid in
609 healthy and diseased airways. *Am. Rev. Respir. Dis.* **148**, 1633-1637 (1993).
610 52 Silver, L. L. Challenges of antibacterial discovery. *Clin. Microbiol. Rev.* **24**, 71-109, (2011).
611 53 Evans, M. E., Feola, D. J. & Rapp, R. P. Polymyxin B sulfate and colistin: Old antibiotics for
612 emerging multiresistant Gram-negative bacteria. *Ann. Pharmacother.* **33**, 960-967
613 (1999).
614 54 Langan, K. M., Kotsimbos, T. & Peleg, A. Y. Managing *Pseudomonas aeruginosa*
615 respiratory infections in cystic fibrosis. *Curr. Opin. Infect. Dis.* **28**, 547-556 (2015).
616 55 Liu, Y.-Y. *et al.* Emergence of plasmid-mediated colistin resistance mechanism MCR-1 in
617 animals and human beings in China: a microbiological and molecular biological study.
618 *Lancet Infect. Dis.* **16**, 161-168 (2016).
619 56 Falagas, M. E., Rafailidis, P. I. & Matthaiou, D. K. Resistance to polymyxins: Mechanisms,
620 frequency and treatment options. *Drug Resist. Update* **13**, 132-138 (2010).
621 57 Moffatt, J. H. *et al.* Colistin resistance in *Acinetobacter baumannii* is mediated by
622 complete loss of lipopolysaccharide production. *Antimicrob. Agents Chemother.* **54**,
623 4971-4977 (2010).
624 58 Pamp, S. J., Gjermansen, M., Johansen, H. K. & Tolker-Nielsen, T. Tolerance to the
625 antimicrobial peptide colistin in *Pseudomonas aeruginosa* biofilms is linked to
626 metabolically active cells, and depends on the *pmr* and *mexAB-oprM* genes. *Mol.*
627 *Microbiol.* **68**, 223-240 (2008).
628 59 Smith, D. J., Anderson, G. J., Bell, S. C. & Reid, D. W. Elevated metal concentrations in the
629 CF airway correlate with cellular injury and disease severity. *J. Cyst. Fibros.* **13**, 289-295
630 (2014).
631 60 Estrela, A. B., Heck, M. G. & Abraham, W.R. Novel approaches to control biofilm
632 infections. *Curr. Med. Chem.* **16**, 1512-1530 (2009).
633 61 Fang, Y. P. *et al.* Multiple steps and critical behaviors of the binding of calcium to
634 alginate. *J. Phys. Chem. B.* **111**, 2456-2462 (2007).
635 62 Hawrani, A., Howe, R. A., Walsh, T. R. & Dempsey, C. E. Thermodynamics of RTA3
636 peptide binding to membranes and consequences for antimicrobial activity. *BBA-*
637 *Biomembranes* **1798**, 1254-1262 (2010).
638 63 Buckner, F. S. & Wilson, A. J. Colorimetric assay for screening compounds against
639 *Leishmania amastigotes* grown in macrophages. *Am. J. Trop. Med. Hyg.* **72**, 600-605
640 (2005).
641 64 Garcia-Gonzalez, L. *et al.* Membrane permeabilization and cellular death of *Escherichia*
642 *coli*, *Listeria monocytogenes* and *Saccharomyces cerevisiae* as induced by high pressure
643 carbon dioxide treatment. *Food Microbiol.* **27**, 541-549 (2010).
644 65 Ghosh, A. *et al.* Sequence context induced antimicrobial activity: insight into
645 lipopolysaccharide permeabilization. *Mol. Biosyst.* **10**, 1596-1612 (2014).
646 66 Culligan, E. P., Marchesi, J. R., Hill, C. & Sleator, R. D. Combined metagenomic and
647 phenomic approaches identify a novel salt tolerance gene from the human gut
648 microbiorne. *Front. Microbiol.* **5**, 10.3389/fmicb.2014.00189 (2014).
649 67 Bochner, B. R. Global phenotypic characterization of bacteria. *Fems Microbiol. Rev.* **33**,
650 191-205 (2009).
651
652
653 **Acknowledgements**

654 The ILL, ISIS and Science and Technology Facilities Council (STFC) are gratefully acknowledged
655 for provision of neutron beamtime and consumables support. We thank Manal AbuOun at
656 the Veterinary Laboratories Agency, Addlestone, Surrey for carrying out the BIOLOG
657 osmolyte assays.

658

659 **Author contributions**

660 E.L.F, D.W.T, K.E.H and P.D.R designed the experiments. L.C.P and M.F.P conducted the AFM
661 imaging. AFM was provided by C.W. S.K., C.E.D., E.L.F. and M.F.P performed and analysed the
662 cell permeability assays. ELS and turbidity assays were carried out by L.C.P, E.L.F. and M.F.P.
663 Osmolyte assays were conducted by S.K. and analysed by K.E.H. and M.F.P. SANS was
664 conducted by P.C.G., E.L.F., R.S., O.M., and M.F.P. CD was carried out by M.F.P. and K.B. ITC
665 experiments were carried out by M.F.P. and N.J.B. All authors discussed the results and
666 commented on the manuscript.

667

668 **Additional information**

669 **Supplementary information** accompanies this paper at http://www.nature.com/
670 scientificreports

671 **Competing financial interests:** This work was funded by AlgiPharma AS, a KESS scholarship and
672 an STFC research grant (SANS).

673

674 **Figure legends:**

675 **Figure 1. Comparison of the effect of OligoG CF-5/20 on Gram-positive and Gram-negative**
676 **bacteria.** Diagram representing the cell wall of (a) Gram-positive and (b) Gram-negative bacteria.
677 Atomic force microscopy (AFM) images of *S. mutans* ± 7 mg/ml OligoG CF-5/20 and *P. aeruginosa* ± 5
678 mg/ml OligoG CF-5/20 at (c) 20 μm^2 and (d) 5 μm^2 (*S. mutans*) and 4 μm^2 (*P. aeruginosa*).

679

680

681 **Figure 2. The effect of OligoG CF-5/20 on bacterial cell membrane permeabilisation.** Cell
682 permeability assay showing (**a**) release of carboxyfluorescein (Cbfl) from single lamellar liposomes
683 composed of egg PC:PG (80:20) in the presence of RTA3 (0.5 µM; positive control) or OligoG CF-5/20
684 at 20-100 mg/ml (**b**) zoomed-in graph of OligoG CF-5/20 only data. Internalisation of (**c**) propidium
685 iodide (PI) and (**d**) nitrocefin (NFN) by PAO1 compared to EDTA (positive) control (1 mM-20 mM). (**e**)
686 Internalisation of 1-N-phenylnaphthylamine (NPN) dye by *P. aeruginosa* strains; PAO1, V2 and
687 NH57388A ± 2-20 mg/ml OligoG CF-5/20 and polymyxin B (positive control). (AU = arbitrary units).
688 (Data represents mean ± SD; ****p*<0.01 and ******p*<0.0001 compared to control; n = 3).

689

690

691 **Figure 3. Effect of OligoG CF-5/20 on *Pseudomonas aeruginosa* PAO1 under various osmolyte**
692 **conditions and on lipopolysaccharide (LPS from *P. aeruginosa*).** Biolog metabolomic osmolyte
693 assay (PM9) representing PAO1 ± 20-100 mg/ml OligoG CF-5/20 (**a**) 4% urea (**b**) 20 mM sodium
694 benzoate pH 5.2 (48 h). (**c**) Precipitation of LPS from *P. aeruginosa* (5 mg/ml) ± 2-20 mg/ml
695 OligoG CF-5/20 or 4 mg/ml colistin sulphate (positive control). (Data represents mean ± SD, n =
696 3). (**d**) Mean zeta potential measurements of 2 mg/ml OligoG CF-5/20 and 10 mg/ml LPS in 0.01
697 M NaCl buffer at pH 5, 7 and 9.

698

699

700 **Figure 4. Structural analysis of LPS ± OligoG CF-5/20.** Small-angle neutron scattering from LPS
701 (10 mg/ml) in D_2O containing 0.001 to 0.1 M NaCl at pH 7 (**a**) alone and (**b**) following incubation
702 (3 h at 37 °C) with OligoG CF-5/20 (20 mg/ml). Circular dichroism spectra of LPS (10 mg/ml) and
703 OligoG CF-5/20 (20 mg/ml) in 0.1 M NaCl at (**c**) pH 5 and (**d**) pH 7 were recorded at 37°C. OligoG
704 CF-5/20 spectra in the absence and presence of 10 mg/ml LPS are shown in blue and red,
705 respectively; the difference of the spectra is shown in green.

706

707 **Figure 5. LPS analysis in the presence of divalent cations**. (**a**) Small-angle neutron scattering (SANS)
708 analysis of LPS (10 mg/ml) and OligoG CF-5/20 (20 mg/ml) in the presence of 5 or 10 mM Ca^{2+} in 0.01
709 or 0.10 M NaCl at pH 7. (**b**) Circular dichroism spectra of 20 mg/ml OligoG CF-5/20 in the presence of

710 10 mg/ml LPS in 0.10 M NaCl were recorded in the presence and absence of 5 mM Ca^{2+} at pH 5 and
711 pH 7 at 37°C; buffer spectra including LPS were subtracted.

712

713 **Figure 6. Interaction between OligoG CF-5/20 and LPS.** (**a**) heat effects per injection (q_i) for the
714 titration of 20 mg/ml OligoG CF-5/20 into 10 mg/ml LPS (▪), 20 mg/ml OligoG CF-5/20 into buffer (o),
715 buffer into 10 mg/ml LPS (Δ), and buffer into buffer (∇) at 37 °C (buffer is 20 mM phosphate pH 7,
716 100 mM NaCl, 1 mM EDTA). (**b**) heat effects per injection (q_i) for the titration of 20 mg/ml OligoG CF-
717 5/20 into 10 mg/ml LPS (▪), 20 mg/ml OligoG CF-5/20 into buffer (o), buffer into 10 mg/ml LPS (Δ),
718 and buffer into buffer (∇) at 37 °C (buffer is 20 mM phosphate pH 7, 100 mM NaCl, 1 mM EDTA.

719

720 **Table legends:**

721 **Table 1. Structural parameters of LPS assuming spherical micelles (radius R_1) and unilamellar**
722 **vesicles (radius R_2 and lamellae thickness).***The mass fraction and composition of materials have
723 been constrained to physically reasonable values in the fitting routine. The concentrations of LPS
724 and OligoG CF-5/20 were 10 and 20 mg/ml, respectively. †A vesicular structure model, looking at the
725 absolute scattering intensities, was utilised (as previously concluded by Bello *et al*. 2014)
726

LPS in D_2O, pH7	**R_1 (±5) / Å**	**R_2 (±10) / Å**	**Thickness (±5) / Å**
LPS, no salt†	n/a	1150	40
1 mM NaCl	22	710	45
1 mM NaCl + OligoG	21	709	45
10 mM NaCl	22	710	46
10 mM NaCl + OligoG	22	709	46
100 mM NaCl	23	710	46

100 mM NaCl + OligoG	21	712	46
10 mM NaCl + OligoG, 5 mM Ca^{2+}†	n/a	1150	45
10 mM NaCl + OligoG, 10 mM Ca^{2+}†	n/a	1150	45
100 mM NaCl + OligoG, 5 mM Ca^{2+}†	n/a	1150	43
100 mM NaCl + OligoG, 10 mM Ca^{2+}†	n/a	1150	48

727

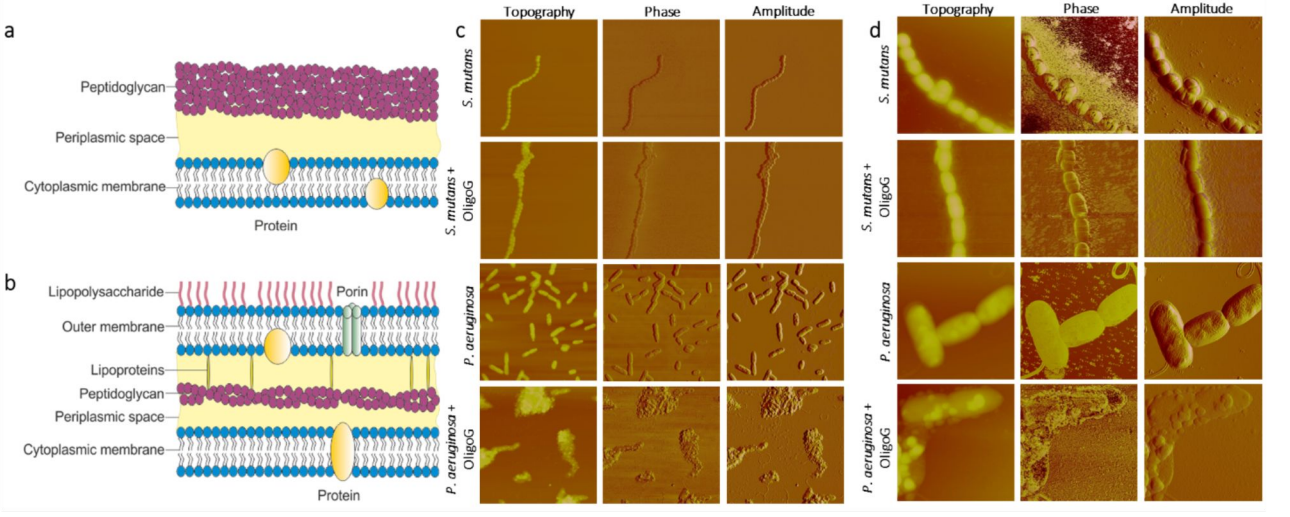
a
Peptidoglycan
Periplasmic space
Cytoplasmic membrane
Protein
b
Lipopolysaccharide
Porin
Outer membrane
Lipoproteins
Peptidoglycan
Periplasmic space
Cytoplasmic membrane
Protein
c
Topography
Phase
Amplitude
S. mutans
S. mutans + OligoG
P. aeruginosa
P. aeruginosa + OligoG
d
Topography
Phase
Amplitude
S. mutans
S. mutans + OligoG
P. aeruginosa
P. aeruginosa + OligoG

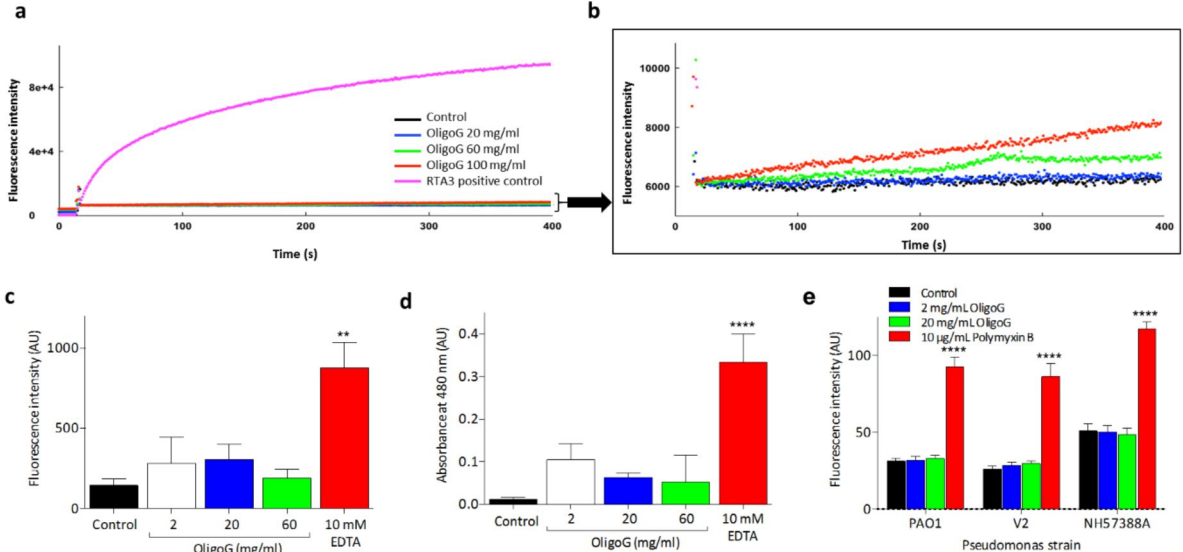
a
Fluorescence intensity
8e+4
4e+4
0
0
100
200
300
400
Time (s)
Control
OligoG 20 mg/ml
OligoG 60 mg/ml
OligoG 100 mg/ml
RTA3 positive control
b
Fluorescence intensity
10000
8000
6000
0
100
200
300
400
Time (s)
c
Fluorescence intensity (AU)
1000
500
0
**
Control
2
20
60
10 mM EDTA
OligoG (mg/ml)
d
Absorbance at 480 nm (AU)
0.4
0.3
0.2
0.1
0.0
****
Control
2
20
60
10 mM EDTA
OligoG (mg/ml)
e
Control
2 mg/mL OligoG
20 mg/mL OligoG
10 µg/mL Polymyxin B
Fluorescence intensity (AU)
100
50
0
****
****
****
PAO1
V2
NH57388A
Pseudomonas strain

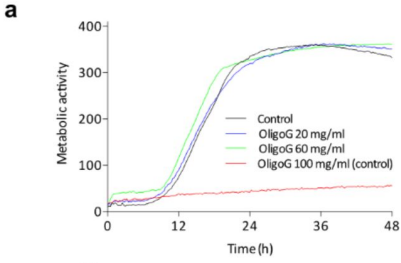

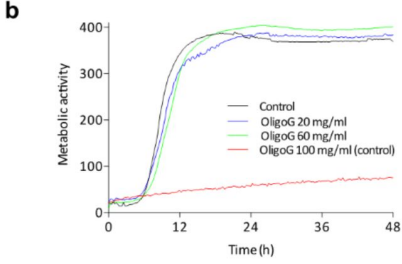

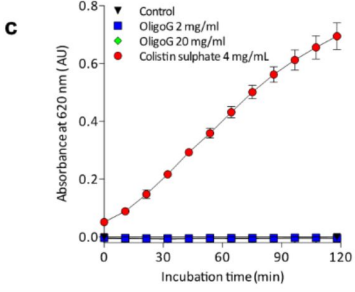

d

	Mean Zeta Potential (mV) ± SD		
pH	**LPS**	**OligoG CF-5/20**	**LPS + OligoG CF-5/20**
5	-40.4 ± 2.8	-28.6 ± 9.7	-37.7 ± 2.4
7	-36.0 ± 1.8	-41.7 ± 4.0	-36.5 ± 2.6
9	-36.3 ± 3.7	-40.0 ± 4.1	-37.7 ± 2.5

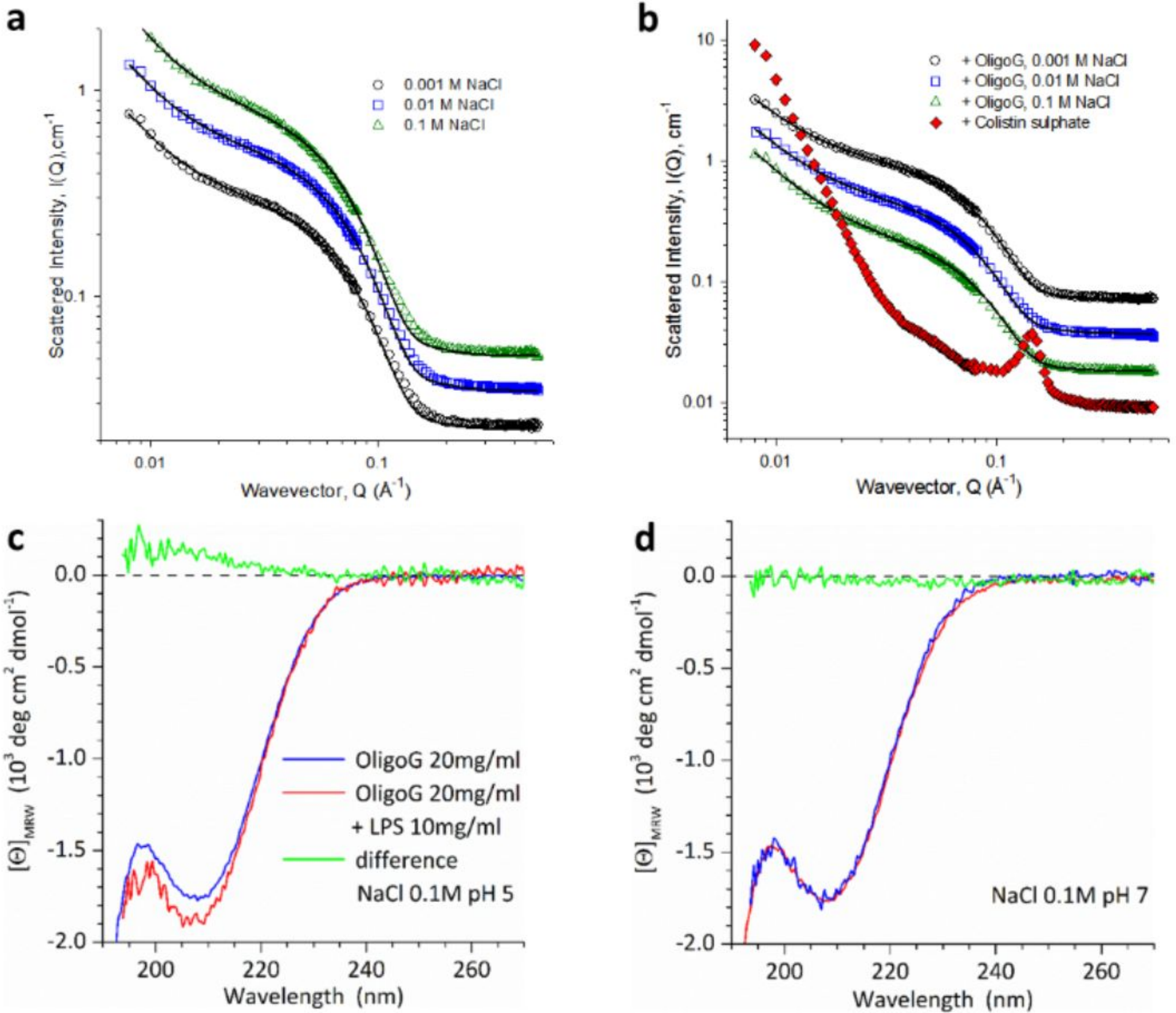
a
0.001 M NaCl
0.01 M NaCl
0.1 M NaCl
Scattered Intensity, I(Q),cm-1
Wavevector, Q (Å-1)
b
+ OligoG, 0.001 M NaCl
+ OligoG, 0.01 M NaCl
+ OligoG, 0.1 M NaCl
+ Colistin sulphate
Scattered Intensity, I(Q), cm-1
Wavevector, Q (Å-1)
c
OligoG 20mg/ml
OligoG 20mg/ml
+ LPS 10mg/ml
difference
NaCl 0.1M pH 5
[Θ]MRW (10³ deg cm² dmol⁻¹)
Wavelength (nm)
d
NaCl 0.1M pH 7
[Θ]MRW (10³ deg cm² dmol⁻¹)
Wavelength (nm)

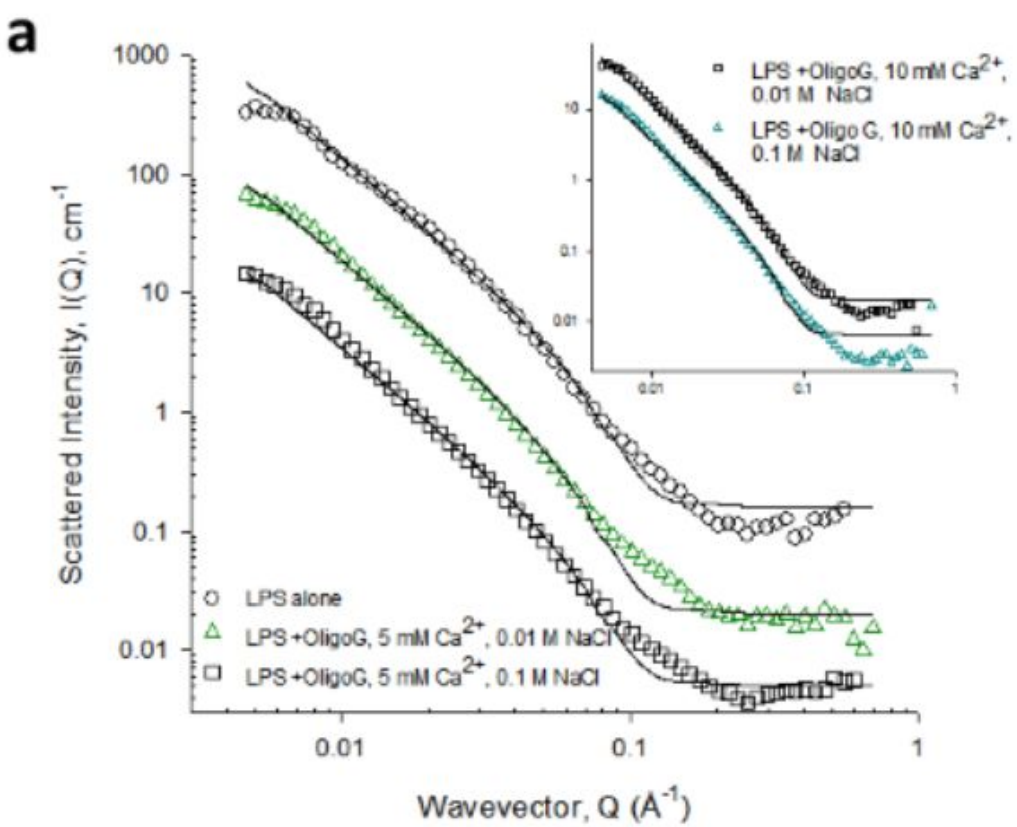
a
Scattered Intensity, I(Q), cm-1
Wavevector, Q (Å-1)
LPS alone
LPS +OligoG, 5 mM Ca2+, 0.01 M NaCl
LPS +OligoG, 5 mM Ca2+, 0.1 M NaCl
LPS +OligoG, 10 mM Ca2+, 0.01 M NaCl
LPS +Oligo G, 10 mM Ca2+, 0.1 M NaCl

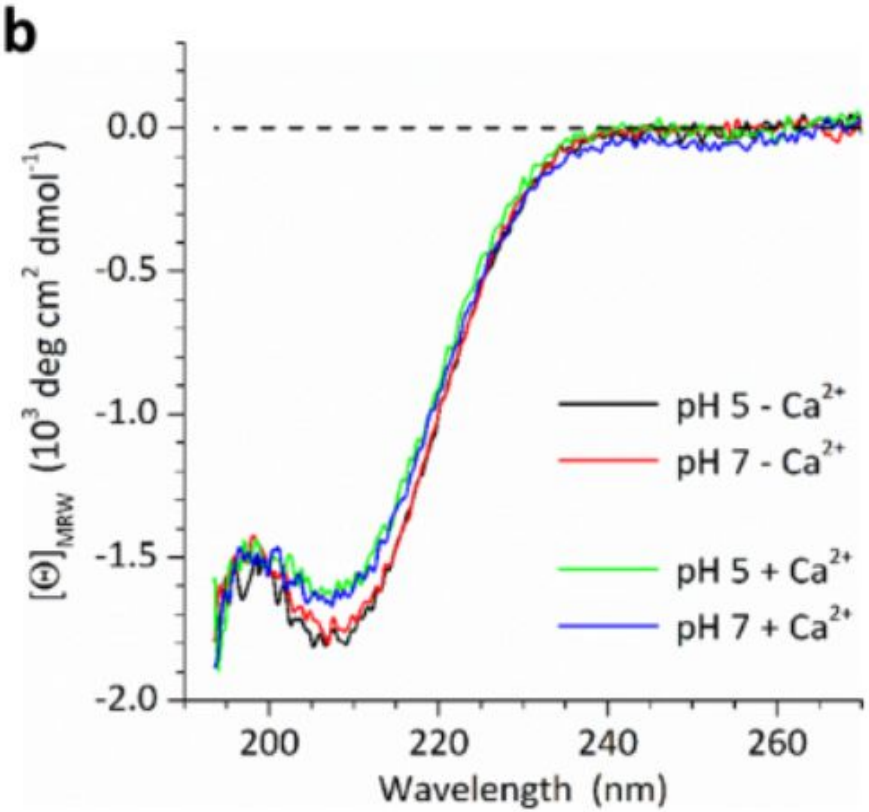
b
[Θ]MRW (10³ deg cm² dmol⁻¹)
Wavelength (nm)
pH 5 - Ca2+
pH 7 - Ca2+
pH 5 + Ca2+
pH 7 + Ca2+

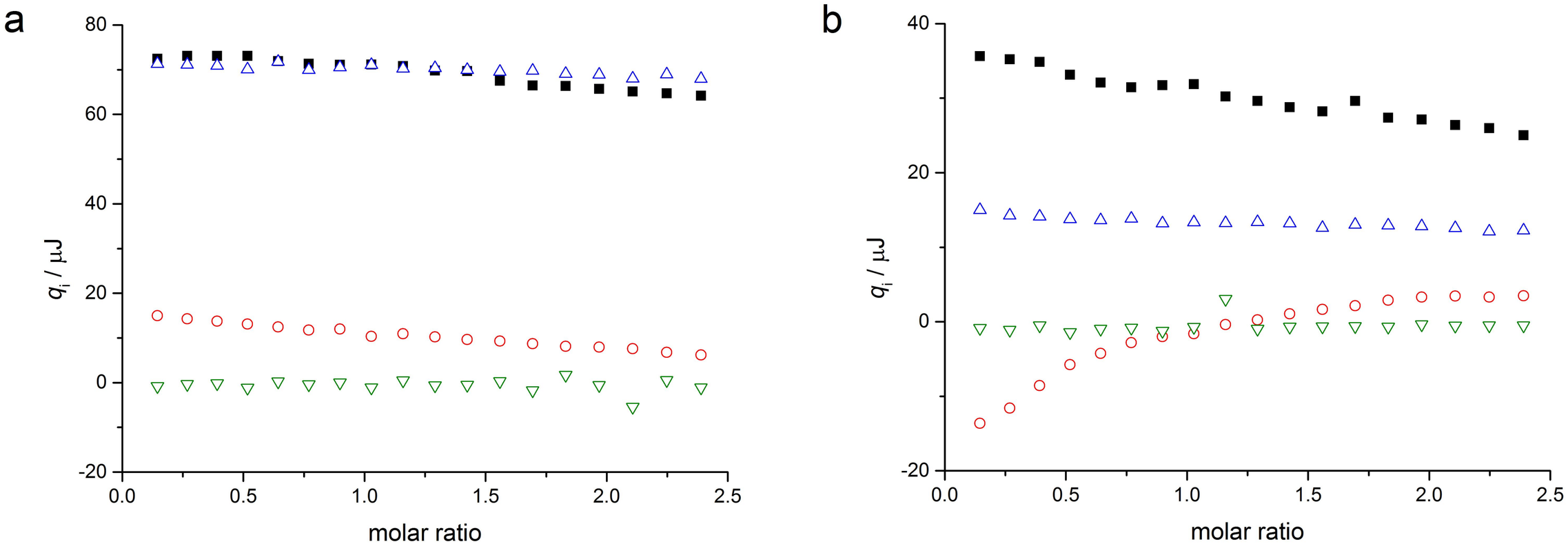
a
80
60
40
20
0
-20
q_i / µJ
0.0
0.5
1.0
1.5
2.0
2.5
molar ratio
b
40
20
0
-20
q_i / µJ
0.0
0.5
1.0
1.5
2.0
2.5
molar ratio